Medium-Cycle Fatigue Behavior of Three Metallic Materials and a Welded Steel Following Gaseous Hydrogen Soaking

KUFOIN, E., BANNISTER, A., BROWN, M., ENGELBERG, D., KAHLON, N., SCENINI, F., ZHOU, Y. <http://orcid.org/0000-0001-6513-7460> and SUSMEL, Luca <http://orcid.org/0000-0001-7753-9176>

Fatigue & Fracture of Engineering Materials & Structures

WILEY

FFEMS Fatigue & Fracture of Engineering Materials & Structures

ORIGINAL ARTICLE OPEN ACCESS

Medium-Cycle Fatigue Behavior of Three Metallic Materials and a Welded Steel Following Gaseous Hydrogen Soaking

E. Kufoin[1] | A. Bannister[2] | M. Brown[2] | D. Engelberg[3] | N. Kahlon[4] | F. Scenini[3,5] | Y. Zhou[3,6] | L. Susmel[7]

[1]Rolls Royce PLC, Derby, UK | [2]Health and Safety Executive (HSE), Science and Research Centre, Buxton, UK | [3]Corrosion@Manchester, Department of Materials, The University of Manchester, Manchester, UK | [4]Progressive Energy Ltd, Stonehouse, UK | [5]Royce Institute, The University of Manchester, Manchester, UK | [6]Laboratory of Advanced Materials of Ministry of Education School of Materials Science and Engineering, Tsinghua University, Beijing, China | [7]School of Engineering and Built Environment, Sheffield Hallam University, Sheffield, UK

Correspondence: L. Susmel (l.susmel@shu.ac.uk)

Received: 17 February 2026 | **Revised:** 2 March 2026 | **Accepted:** 9 March 2026

Keywords: hydrogen | medium-cycle fatigue | metallic materials

ABSTRACT

This study investigates the impact of hydrogen soaking on the medium-cycle fatigue behavior of various metallic materials commonly used in gas transmission pipelines. The tested materials include ex-service gray cast iron, ex-service X52 carbon steel, brass, and welded X52 carbon steel. A comprehensive fatigue testing program was conducted on both as-received and hydrogen-soaked specimens. Rigorous statistical analysis of the results revealed minimal impact of hydrogen on fatigue life for the materials and hydrogen charging conditions studied. The experimental data for hydrogen-soaked specimens aligned closely with baseline scatter bands from as-received specimens. This work suggests that, for the specific hydrogen-charging procedure and fatigue testing conditions employed, additional considerations for hydrogen effects in fatigue design may not be necessary for the materials examined.

1 | Introduction

Hydrogen, as a versatile and clean-burning energy carrier, is increasingly recognized as a vital solution for reducing greenhouse gas emissions and facilitating the transition to a more sustainable energy future. With its ability to power a diverse range of applications across multiple sectors, such as transportation, industry, and residential heating, hydrogen presents a compelling and eco-friendly alternative to traditional fossil fuels [1]. As the world seeks cleaner energy sources, hydrogen offers a scalable and adaptable solution that could play a pivotal role in achieving net-zero emissions goals.

One particularly promising application of hydrogen is its integration into the existing natural gas infrastructure [2]. In the recent past, hydrogen blending was widely regarded as a practical and economically attractive pathway for decarbonizing the gas network. By introducing relatively low concentrations of hydrogen into the existing natural gas infrastructure, it was believed that significant reductions in carbon emissions could be achieved without the need for extensive or costly modifications to pipelines, appliances, or distribution systems. Blending was therefore presented as a cost-effective and operationally straightforward means to support the transition toward a low-carbon energy system, while preserving the functionality of the established gas network and enabling a gradual increase in hydrogen concentrations over time. However, more recent developments have reshaped this narrative. International policies and industry assessments increasingly indicate that hydrogen is unlikely to play a major role in decarbonizing domestic space heating, where heat pump technologies are now viewed as the preferred long-term solution. As a result, the perceived value

Summary

- Hydrogen presoaking had a negligible effect on medium-cycle fatigue of pipeline metals.
- Fatigue performance of soaked specimens stayed within as-received scatter bands.
- Variations in fatigue parameters depend on soaking time and sample size differences.
- No additional design allowances for hydrogen are needed under studied conditions.

of hydrogen blending as a transitional measure for household heating has diminished. Instead, the primary strategic driver for hydrogen production has shifted toward industrial decarbonization, particularly in conjunction with carbon capture and storage infrastructure. Within this context, hydrogen blending remains important mainly as a mechanism to provide a stable offtake for early large-scale hydrogen production facilities, thereby supporting their commercial viability. Consequently, the role of blending is evolving from an enabler of domestic heating decarbonization to an instrument that underpins the broader industrial hydrogen economy.

Nevertheless, the successful implementation of hydrogen blending depends on a comprehensive understanding of how hydrogen interacts with existing infrastructure components [3]. Hydrogen possesses distinct physical and chemical properties that differ from natural gas, which necessitates careful consideration of its effects on pipeline materials, fittings, valves, and end-use appliances. Issues such as hydrogen embrittlement, material degradation, and seal compatibility must be thoroughly assessed to maintain the integrity, safety, and reliability of the gas network [4, 5].

Conducting rigorous testing and evaluation of these factors will be critical to ensuring that the gas infrastructure can handle hydrogen blending without compromising performance or safety. By addressing these challenges, we can confidently move forward with the integration of hydrogen as a clean energy source, safeguarding the functionality of existing infrastructure while making significant progress in reducing greenhouse gas emissions.

Since the late 19th century [6], extensive research has been devoted to examining the impact of hydrogen on metals. These studies have highlighted significant challenges to structural integrity, including hydrogen embrittlement, reduced fracture toughness, and diminished fatigue resistance. In this context, a detailed review and analysis of the state-of-the-art literature [7–35] have been conducted, and the most significant findings can be summarized as follows:

- The presence of hydrogen gas has only a minimal effect on yield stress, ultimate tensile strength, and fatigue endurance limit [10, 36–39].
- In contrast, elongation at failure, fracture toughness, and resistance to fatigue crack propagation are significantly reduced in hydrogen-rich environments [40–42].

With specific reference to fatigue, the available technical literature appears to converge on a number of widely accepted conclusions [7–42], which can be summarized as follows:

- Crack growth rates increase in the presence of pure hydrogen gas [21, 22].
- The detrimental effect of hydrogen gas on fatigue crack behavior is influenced by several factors that include the microstructural characteristics of the metallic material, exposure temperature and pressure conditions, and the frequency of the applied load [11, 19, 22, 30].
- Regarding crack initiation, hydrogen appears to have a slight impact on medium-cycle fatigue performance [10, 14]. However, a review of existing studies reveals that no comprehensive statistical investigation has yet been conducted to quantify the effect of hydrogen in the medium-cycle fatigue regime rigorously.
- In high-cycle fatigue, the influence of hydrogen on the crack initiation process is so minor that it can generally be neglected without compromising accuracy [25, 35].
- The above observations regarding crack initiation also seem to apply to metallic materials with stress concentrators [24].
- Fretting fatigue strength is notably reduced in the presence of hydrogen, which could pose significant challenges in applications involving mechanical joints [9, 12].

While the above considerations aim to reflect the current state of knowledge, it must be acknowledged that drawing definitive conclusions is challenging. This difficulty arises because the outcomes of experimental studies investigating the effects of hydrogen can also depend on the specific hydrogen exposure techniques employed [34, 43].

In metal pipelines conveying hydrogen-blended gas, hydrogen atoms are generated at the gas/metal interface and diffuse into the metal lattice, creating a through-thickness concentration gradient rather than an immediately uniform bulk concentration. The process begins when molecular hydrogen dissociates at the internal surface; the resulting atomic hydrogen first adsorbs onto the metal surface and is then absorbed into interstitial lattice sites, from where it diffuses inward with a flux proportional to the concentration gradient and the material's diffusivity. At the same time, microstructural traps (such as dislocations, carbides, and grain boundaries) capture hydrogen and modify both the effective diffusible fraction and the spatial profile. For pipeline geometries and service times of practical interest, this results in a depth-dependent hydrogen chemical potential and a nonuniform distribution strongly influenced by pressure, temperature, surface condition, and trap density.

In laboratory studies, various charging methods can be used to introduce hydrogen into a specimen. Once hydrogen is absorbed into the metal lattice, its effect on mechanical behavior does not depend on the entry route [44]. However, the charging technique strongly influences the amount of hydrogen uptake, its spatial distribution, and the presence of traps, which in turn affects experimental outcomes. For example, electrochemical (cathodic) charging introduces hydrogen by reduction at the specimen

surface in an aqueous electrolyte, creating a high surface activity that drives inward diffusion. Under typical conditions for small specimens and sufficiently long charging times, this can lead to a nearly uniform diffusible hydrogen concentration, especially if postcharging equilibration is allowed. In contrast, service exposure often involves ingress from one side of a thick wall, producing persistent gradients.

In situ mechanical testing in gaseous hydrogen environments provides a different experimental boundary condition by maintaining an external hydrogen partial pressure during loading. Methods such as hollow-specimen tensile rigs, small high-pressure chambers, or purpose-designed fixtures allow tests at controlled hydrogen pressures and temperatures while the mechanical load is applied; the specimen therefore experiences an ongoing external source of hydrogen during deformation. For thin or purposely hollowed specimens, the continuous supply of hydrogen can lead to relatively rapid equilibration and a near-steady hydrogen concentration during the test, but for more representative section thicknesses, the through-thickness profile will still reflect the interplay of gas pressure, diffusivity, loading duration, and trapping kinetics. Importantly, in situ testing reproduces the simultaneous presence of an external hydrogen fugacity and applied stress, so that phenomena dependent on concurrent adsorption/diffusion and stress (e.g., hydrogen flux to a propagating crack tip) can be observed directly [45–47].

Precharging to steady state in gaseous hydrogen followed by immediate ex situ testing represents a further, distinct experimental condition that isolates the influence of hydrogen retained in the bulk from the influence of a continuing external source. When specimens are exposed to hydrogen at elevated pressure for long enough to approach local equilibrium (or to fill available traps), the hydrogen distribution within the material may reach a steady state governed by the test conditions; removing the specimen from the pressure vessel and testing it ex situ examine mechanical response when the external fugacity is withdrawn but the internal, trapped and/or dissolved hydrogen remains. The mechanical consequences of hydrogen present prior to loading (pre-charged, ex situ) can differ markedly from those observed when hydrogen is supplied continuously during loading (in situ): effects on yield behavior, ductility, crack initiation, and fatigue crack growth rates may be sensitive to whether hydrogen is being delivered during deformation versus being already resident in traps or lattice sites [48]. Thus, an experimental program that deliberately saturates specimens with gaseous hydrogen and then conducts ex situ fatigue tests probes the damage mechanisms and kinetics relevant to materials containing retained hydrogen (e.g., after pressurized service or rapid decompression) rather than the coupled diffusion-during-loading phenomena that in situ gas tests reveal [49]. This is the rationale behind the present investigation.

Hydrogen retained in metals—even in the absence of ongoing charging while cyclic loading is applied—can reduce fatigue life in the medium-cycle fatigue regime [35] and accelerate fatigue crack growth [3]. The severity of these effects depends on material class, hydrogen concentration, microstructure, and loading conditions. Most studies report detrimental outcomes [50–52], although some mitigating factors (e.g., hydrogen-trapping precipitates) have been documented [53, 54]. The proposed mechanisms include hydrogen-enhanced localized plasticity, hydride formation, and alterations in both crack initiation and propagation modes, all of which influence fatigue performance.

Taken together, these considerations explain why different laboratory hydrogenation methods are not interchangeable: through-thickness gradients arising from one-sided permeation in service, the degree of homogenization achievable with cathodic charging, the continuous-supply conditions of in situ gaseous tests, and the retained-hydrogen state produced by saturation-then-ex situ testing each establish distinct initial and boundary conditions that control hydrogen availability at microstructural traps and crack tips. Consequently, interpreting fatigue and fracture data requires careful attention to the charging history, specimen geometry, and trap structure; comparing results across methods without accounting for these differences can obscure our understanding.

While the interplay between cracks or defects and fatigue in metals is well established, a clear gap remains in both data and comprehensive models describing fatigue behavior in the absence of cracks/defects—particularly within continuum-mechanics frameworks [35].

In light of these considerations, this study aims to provide a systematic and statistically robust assessment of how hydrogen exposure influences the medium-cycle fatigue behavior of materials commonly used in gas transmission pipelines. The investigation focuses on ex-service gray cast iron, ex-service X52 carbon steel, brass, and welded X52 steel, comparing their fatigue performance in the as-received condition and after controlled hydrogen presoaking designed to reproduce through-thickness hydrogen-gradient conditions relevant to hydrogen-blended natural-gas pipelines. By combining long-duration hydrogen exposure with rigorous fatigue testing and statistical analysis, this work aims to determine whether hydrogen retention and its gradual release under practical conditions significantly affect fatigue life, thereby addressing the current gap in quantitative data for this scenario. Finally, given the specific requirements of this project, the problem is addressed from a fatigue design perspective rather than through microstructural analyses aimed at elucidating changes in crack initiation and propagation mechanisms.

2 | Materials and Metallurgy

A total of three different metallic materials and one welded steel were tested under two conditions: without hydrogen exposure (baseline) and after hydrogen presoaking. The materials included ex-service gray cast iron (spun cast), ex-service X52 carbon steel, brass, and welded X52 carbon steel. The specimens were manufactured with their axis parallel to the circumferential direction of the pipe, since fatigue cracks in pressurized pipelines generally develop in the longitudinal direction. The welded samples were fabricated in strict accordance with the recommendations of BS 4515-1:2009 and were subsequently ground to create polished, butt-welded dog-bone specimens. No

postweld heat treatment was applied to relieve residual stresses induced by the welding process.

For hydrogen exposure testing and hardness measurements, all sample surfaces were manually ground to a 600-grit SiC finish to remove scale and surface contamination. For microstructural characterization, the cast iron specimens were further ground to 1200-grit and polished using 1-μm diamond paste, whereas the brass and X52 steel specimens were ground to 1200-grit, polished using 0.25-μm diamond paste, and subsequently finished with an oxide polishing suspension (OPS). On the basis of typical roughness levels associated with these preparation routes, the arithmetic mean roughness values were of the order of $Ra \approx 0.1\,\mu m$ for the 600-grit ground surfaces, $Ra \approx 0.02\,\mu m$ after 1200-grit grinding, $Ra \approx 0.01–0.02\,\mu m$ after 1-μm diamond polishing, and $Ra \approx 0.005–0.01\,\mu m$ after 0.25-μm diamond polishing followed by OPS finishing.

All samples were hardness tested using either a Buehler Micromet micro-hardness tester with an applied load of $HV_{0.2}$ or a Struers Durascan 80 with an applied load of $HV_{0.5}$.

Etched microstructural analysis of the ex-service cast iron revealed elongated, winding graphite flakes embedded within a heterogeneous metallic matrix (Figure 1a). The morphology and distribution of these graphite flakes are characteristic of gray cast iron. Energy-dispersive X-ray spectroscopy (EDX) mapping further revealed a complex, multiphase microstructure consisting of ferrite, pearlite (Fe/Fe_3C), graphite flakes, and a phosphorus-containing eutectic phase (steadite). In addition, small, bright particles enriched in manganese and sulfur were detected, indicating the presence of MnS inclusions. The strong microstructural heterogeneity was reflected in a wide scatter of hardness values, ranging from approximately 270–430 HV, with a mean value of about 348 HV, which is fully consistent with the coexistence of soft ferritic regions, harder pearlitic areas, and brittle eutectic constituents.

Optical microscopy of the α-/β-brass revealed a two-phase, zinc-rich alloy microstructure with a mean hardness of 111 HV (Figure 1b). The darker α-phase grains were richer in copper, whereas the lighter β-phase grains contained higher zinc contents, consistent with a duplex brass alloy. Scanning electron microscopy (SEM) coupled with EDX analysis confirmed this phase partitioning and further revealed the presence of small lead-rich particles, which were preferentially located at the α/β phase boundaries. These Pb-rich particles are typical of free-machining brasses and are known to influence local ductility and damage initiation mechanisms, although no macroscopic differences in fracture behavior were observed between hydrogen-exposed and unexposed specimens in this study.

Optical microscopy of the ex-service X52 steel indicated a ferritic–pearlitic microstructure with a mean hardness of 184 HV. Nital etching revealed a pronounced banded microstructure containing pearlite, interphase regions, and grain boundaries, indicative of process-induced orientations associated with the manufacturing route of the material. Larger equiaxed grains were interspersed with regions of finer, elongated grains arranged in parallel bands, suggesting a warm-forming process during pipe production. This processing route resulted in flattened ferrite grains and planar pearlite colonies aligned with the forming direction, as shown in Figure 1c, and is typical of thermo-mechanically processed pipeline steels.

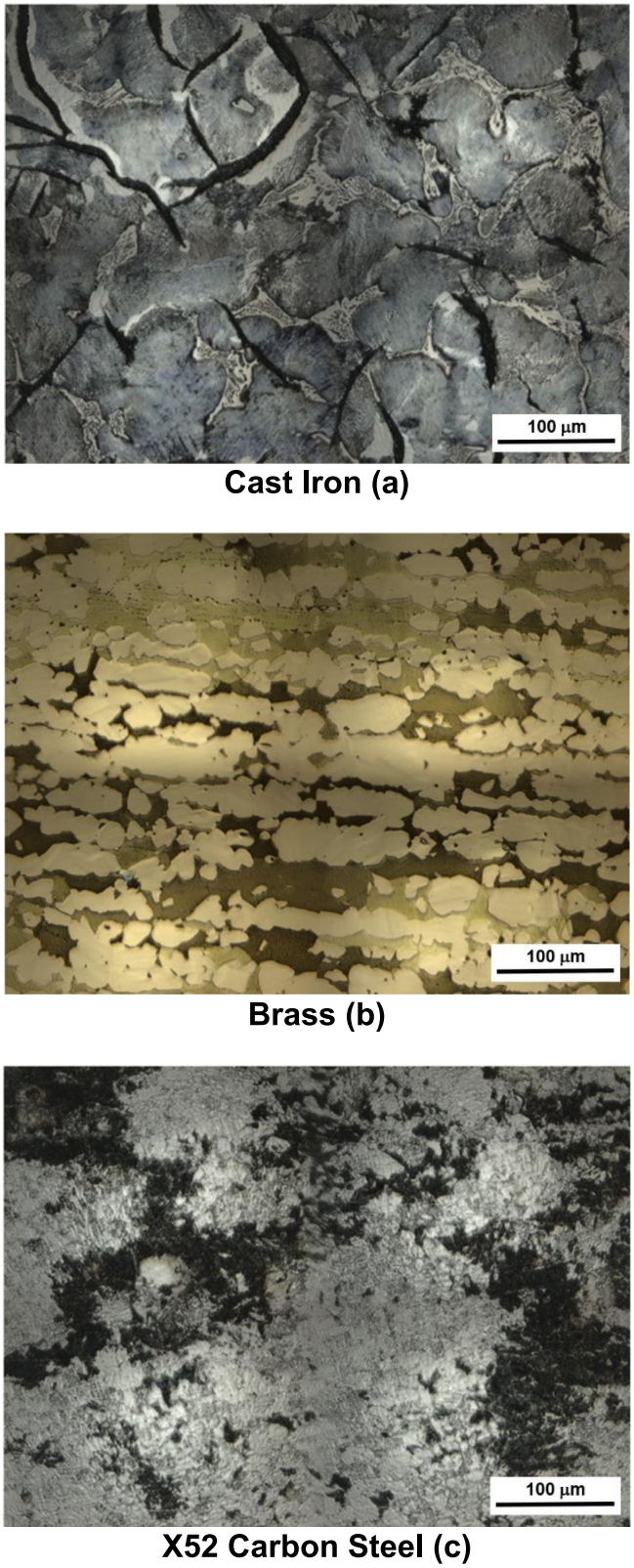

FIGURE 1 | Etched microstructure of the three metallic materials used in the present investigation. [Colour figure can be viewed at wileyonlinelibrary.com]

Microstructural analysis of the welded X52 carbon steel revealed the presence of three distinct regions: the base metal, the heat-affected zone (HAZ), and the weld metal. The base material retained a ferritic–pearlitic microstructure similar to that of the parent X52 steel, while the HAZ exhibited microstructural gradients associated with the welding thermal cycle. The weld region itself was characterized by relatively coarse pearlitic grains, with a generally uniform distribution of pearlite across the substrate. EDX mapping indicated locally elevated concentrations of manganese (Mn) and sulfur (S), consistent with the presence of MnS inclusions, and in some cases also revealed increased aluminum (Al) contents, suggesting the presence of additional inclusion types. Such MnS inclusions are widely recognized as potential initiation sites for hydrogen-assisted cracking and can play a significant role in hydrogen trapping and damage localization. Hardness measurements across the welded joint showed no marked differences between the base metal and the weld region, with a mean hardness of approximately 175 HV, although slightly higher local values (up to about 200 HV) were occasionally observed in the HAZ.

3 | Hydrogen-Soaking and Fatigue Testing

Flanged circular pressure tubes, made from Type 316L stainless steel, were commissioned for hydrogen exposure testing (Figure 2a). These tubes had a length of 1000 mm with a 52-mm internal diameter, providing space to expose several test samples to a pure hydrogen gas environment. The tubes were loaded with test samples, then pressurized with nitrogen gas, emptied, and then thoroughly flushed with nitrogen gas to remove moisture and any potential gas impurities.

Test specimens were placed inside the tubes (Figure 2b) and then exposed to high-purity hydrogen gas at a specified pressure of 8–10 bar and ambient temperature.

A rough estimate of the time required to reach a saturated hydrogen condition was obtained using a simple 1D through-thickness Fickian diffusion model for a flat plate. The specimens were exposed to hydrogen on the two large faces, so the characteristic diffusion length was taken as the half-thickness (i.e., 1 mm). Full saturation was defined as 99% of the through-thickness average concentration. Using representative room-temperature effective diffusion coefficients, D, the resulting diffusion-limited saturation times were about 2 h for ex-service X52 steel ($D = 2.37 \times 10^{-10}\,m^2/s$ [55]), up to 21 days for gray cast iron ($D = 1 \times 10^{-12}\,m^2/s$ [56]), and up to 25 days for brass ($D = 8.2 \times 10^{-13}\,m^2/s$ [57]). For the flush-ground welded X52 steel, the same diffusion-only model would predict saturation on hour-to-day timescales if its effective diffusivity is comparable to that of the base metal (of the order of 10^{-10}–$10^{-9}\,m^2/s$); however, the weld metal/HAZ and the grinding process can introduce microstructural heterogeneity, residual stresses, and strong hydrogen trapping, so the relevant effective D can be orders of magnitude lower and the apparent saturation time correspondingly much longer—meaning that, for welded specimens, these estimates are inherently more uncertain and should be treated as order-of-magnitude only [58]. According to the above theoretical considerations, exposures were carried out for 3–9 months.

After completing the exposure interval, the tubes were purged again with nitrogen gas, and samples retrieved and stored in liquid nitrogen to minimize any potential hydrogen loss via outgassing. To further prevent hydrogen loss during transportation before fatigue testing, the samples were transferred in containers filled with dry ice and subsequently stored in a scientific freezer at −80°C.

Accurate quantification of hydrogen content, particularly at low concentrations or near surfaces, required specialized techniques. At the time of this study, these capabilities were not available in-house, and outsourcing posed a risk of unreliable results due to delays between exposure and measurement. Although

FIGURE 2 | Pressure tubes and gas flow rack for gaseous hydrogen exposure (a); specimens placed inside a pressure tube prior to exposure to hydrogen (b). [Colour figure can be viewed at wileyonlinelibrary.com]

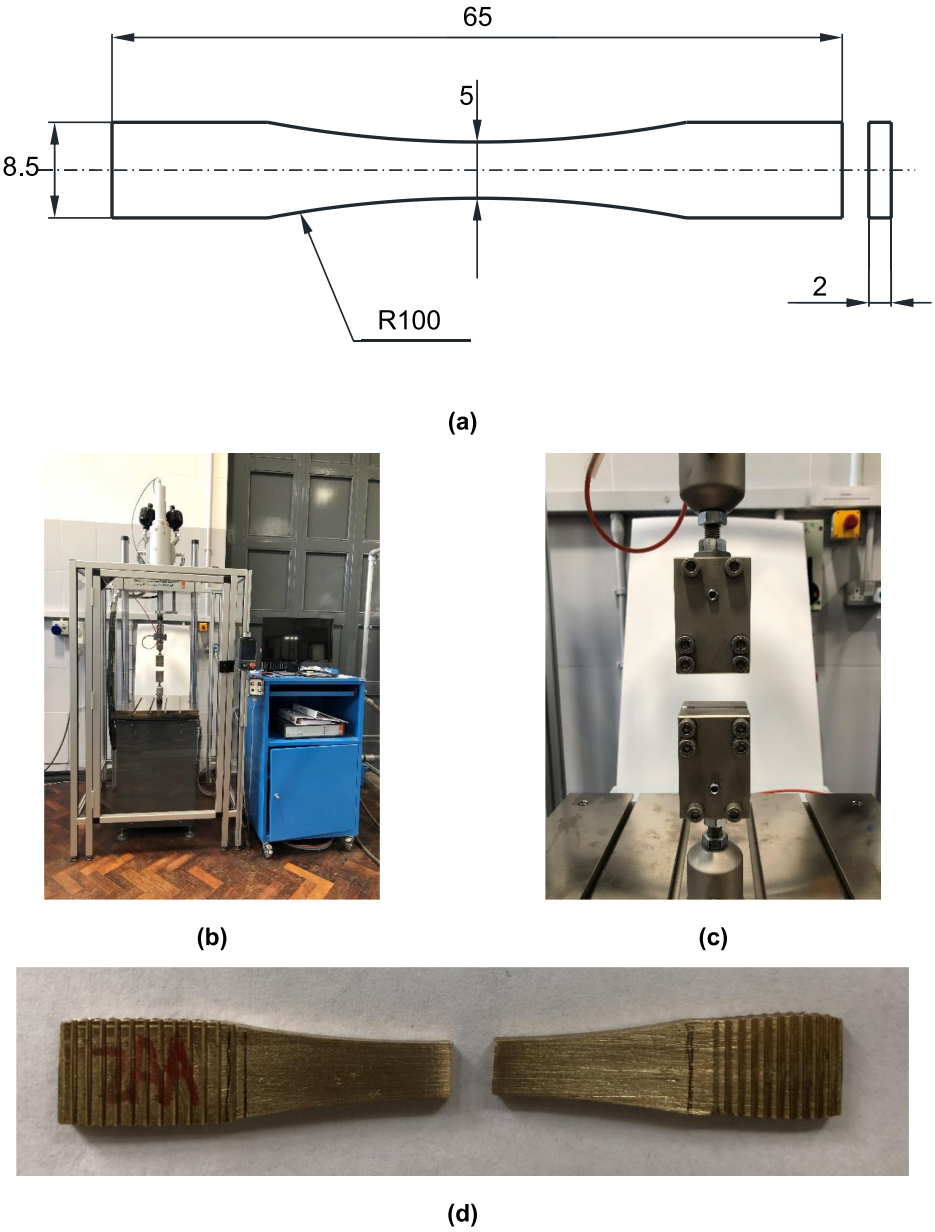

FIGURE 3 | Technical drawing of the fatigue specimen with nominal dimensions in millimeters (a), fatigue testing machine (b), mechanical grips (c), and example of a brass specimen broken under fatigue loading (d). [Colour figure can be viewed at wileyonlinelibrary.com]

preliminary hydrogen concentration data were obtained, they were deemed unreliable and therefore excluded from this analysis. Consequently, hydrogen concentration measurements are not reported here.

To assess the fatigue behavior of the materials of interest, including the welded steel under consideration, fatigue specimens were manufactured as per the technical drawing shown in Figure 3a. The specimen design [59] was optimized to ensure compact dimensions, facilitating effective soaking and easy transport. The dog-bone specimens seen in Figure 3 were designed with a net stress concentration factor, K_t, of 1.01 [60]. For the transversely butt-welded specimens, the welds were ground flush to the plate surface to eliminate any potential effects associated with localized stress concentration phenomena at the weld toes.

Fatigue tests were conducted using a 25-kN servo-hydraulic Walter+Bai fatigue testing machine (Model LFV-25-ME), controlled via the Walter+Bai PCS8000 Digital Controller (Figure 3b). The fatigue tests were performed by clamping the samples using 25-kN fatigue-rated mechanical grips (Figure 3c).

Axial loading fatigue tests were carried out in load control mode at a frequency of 10 Hz. Lower fatigue loading frequencies in the presence of hydrogen promote accelerated crack growth and increased embrittlement, owing to enhanced hydrogen diffusion and accumulation at the crack tip [3, 61]. A testing frequency of 10 Hz represents a practical compromise [47, 61–63]: it is sufficiently high to minimize the duration of fatigue testing while still allowing hydrogen-assisted degradation to be observed in susceptible materials, and it remains representative of pipeline loading conditions [61]. Nevertheless, caution is required when

extrapolating these results to real-world conditions, particularly for components operating at very low frequencies in hydrogen-containing environments [47].

The failure criterion was defined as the complete fracture of the samples, as illustrated in Figure 3d. Owing to the very limited net width of the specimens (5 mm), direct observations by

TABLE 1 | Summary of the generated experimental results in terms of $\Delta\sigma_{0,50\%}$, k, and T_σ for different hydrogen-soaking periods.

Material	Soaking time (months)	Number of specimens	$\Delta\sigma_{0,50\%}$ (MPa)	k	T_σ
Steel	0	18	449.8	53.3	1.057
	3/4	15	445.2	55.7	1.032
	5	15	435.6	36.1	1.097
	9	9	431.6	35.0	1.194
Welded steel	0	15	446.4	46.6	1.139
	3/4	10	364.1	14.7	1.671
	9	7	376.5	14.9	1.417
Cast iron	0	15	61.1	8.2	1.437
	3/4	9	73.5	9.9	1.433
	9	9	85.7	17.3	1.182
Brass	0	10	186.1	6.1	1.468
	9	8	229.1	12.4	1.210

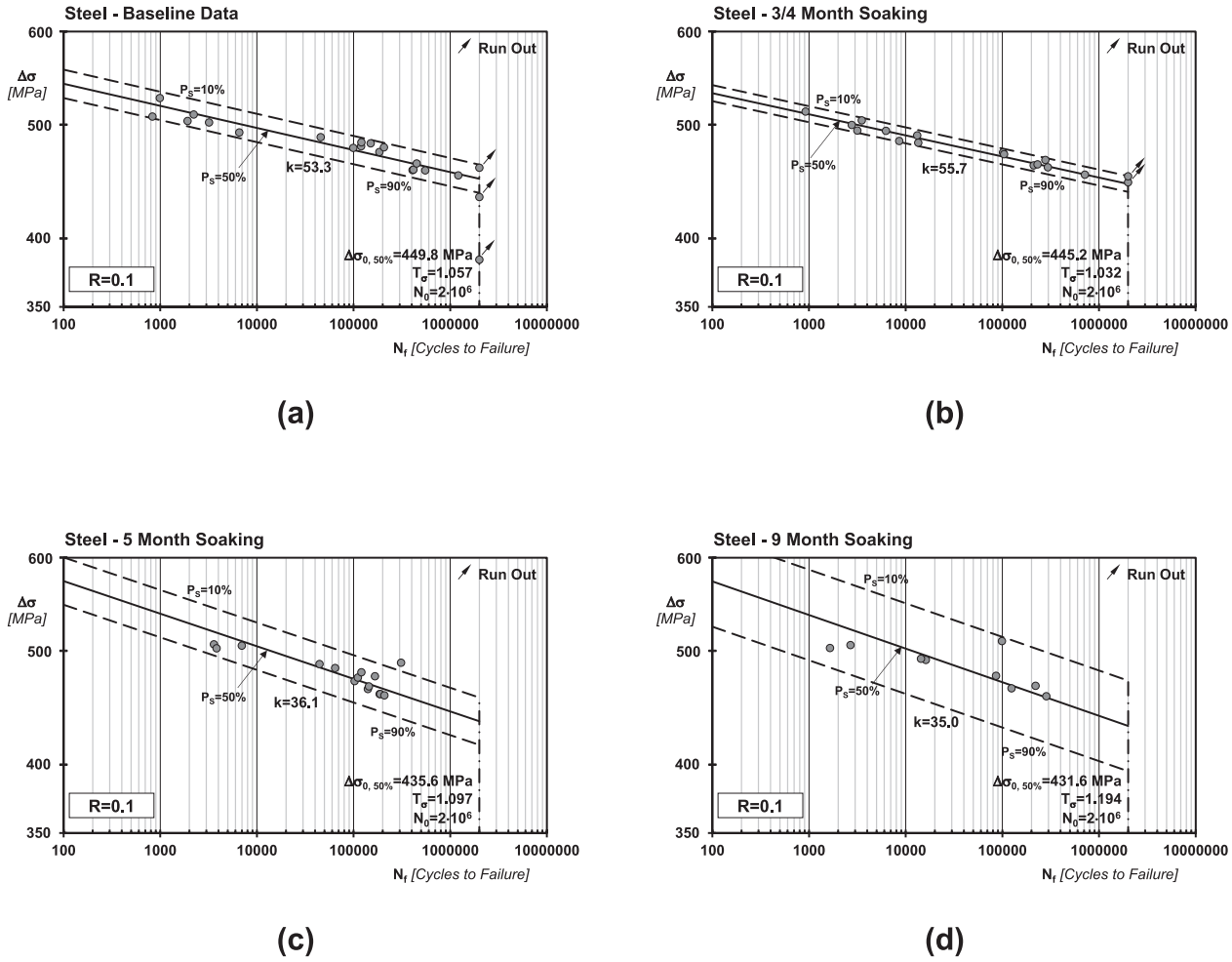

FIGURE 4 | Fatigue results generated by testing un-soaked (a) and hydrogen-soaked specimens (b–d) of X52 carbon steel.

optical microscopy showed that, for these geometries, crack initiation accounted for at least 95%–98% of the total fatigue life, and this behavior was consistently observed for all the materials investigated. Accordingly, the adopted failure criterion can be considered representative of the crack initiation life, with crack propagation contributing only marginally and therefore not significantly affecting the measured fatigue life. Run-out tests were stopped when the number of cycles reached 2×10^6. For the welded specimens, fatigue cracks were observed to initiate and propagate in the HAZ, both in the unsoaked and hydrogen-soaked conditions.

Given that the structural components of gas networks are typically pretensioned, fatigue specimens were tested under a load ratio ($R=\sigma_{min}/\sigma_{max}$) of 0.1. This experimental approach allowed to simulate realistic in-service loading conditions, enabling the investigation of the combined effects of hydrogen and nonzero mean stress. As hydrogen primarily affects the fatigue behavior of metallic materials in the low-to-medium cycle fatigue regime [35], fatigue data were generated within the range of 10^3–2×10^6 cycles to failure.

Since, according to the JSME S 002-81 Standard Method of Statistical Fatigue Testing developed by the Japan Society of Mechanical Engineers, the recommended approach to determining an S–N curve is based on tests of eight specimens, the experimental program was conducted using at least eight samples for each material and condition investigated (see Table 1).

To assess the impact of hydrogen on the fatigue behavior of the investigated materials, including the welded steel, a series of fatigue curves were determined experimentally. Reference (baseline) fatigue curves were generated from unsoaked specimens tested in their as-received condition. Additional curves were generated for specimens soaked in hydrogen for durations ranging from 3 to 9 months.

4 | Fatigue Results: Statistical Reanalyses and S–N Curves

Figures 4–7 present the S–N curves determined by postprocessing the experimental results obtained using the procedure outlined in Section 3. Using the standard approach recommended by ASTM [64], the experimental data were statistically reanalyzed assuming a log-normal distribution of cycles to failure at each stress level, with a 95% confidence level. The results of these analyses are summarized in Figures 4–7 in terms of negative inverse slope, k, endurance limit range, $\Delta\sigma_{0,50\%}$, at 2×10^6 cycles to failure for a probability of survival, P_S, equal to 50%, and scatter ratio of the endurance limit range

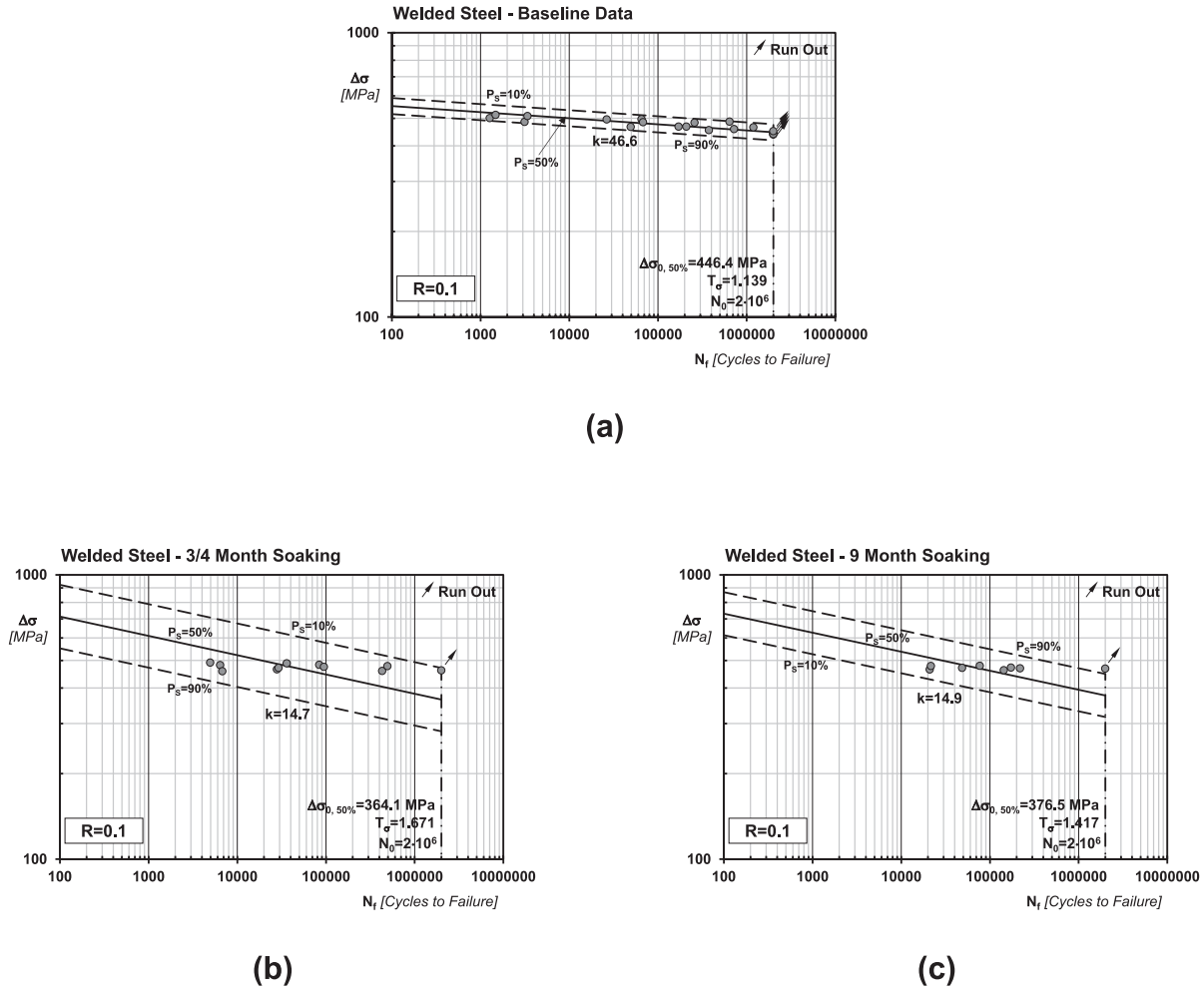

FIGURE 5 | Fatigue results generated by testing unsoaked (a) and hydrogen-soaked specimens (b, c) of welded X52 carbon steel.

(at 2×10^6 cycles to failure) for 90% and 10% survival probabilities, T_σ [65, 66]. These statistical analysis results are also reported in Table 1.

The results from testing as-received and 3/9 months hydrogen soaked X52 specimens reveal several key findings. First, the S–N curves generated for both types of specimens (see Figure 4 and Table 1) exhibit exceptionally high negative inverse slope values, ranging from 35.0 to 55.7. These values are significantly larger than those typically observed in conventional metallic materials, which usually display k values between 8 and 12 [67]. Second, the level of scatter in the data tends to increase slightly with longer soaking times. Third, according to Table 1, both $\Delta\sigma_{0,50\%}$ and k decrease with increasing soaking time, with the reduction in endurance limit for a 9-month soaking period being approximately 4.2%. Having observed these relevant aspects, it is important to conclude by noting that the trends observed in Table 1 for steel are influenced not only by the hydrogen-soaking process but also by the varying sizes of the statistical samples.

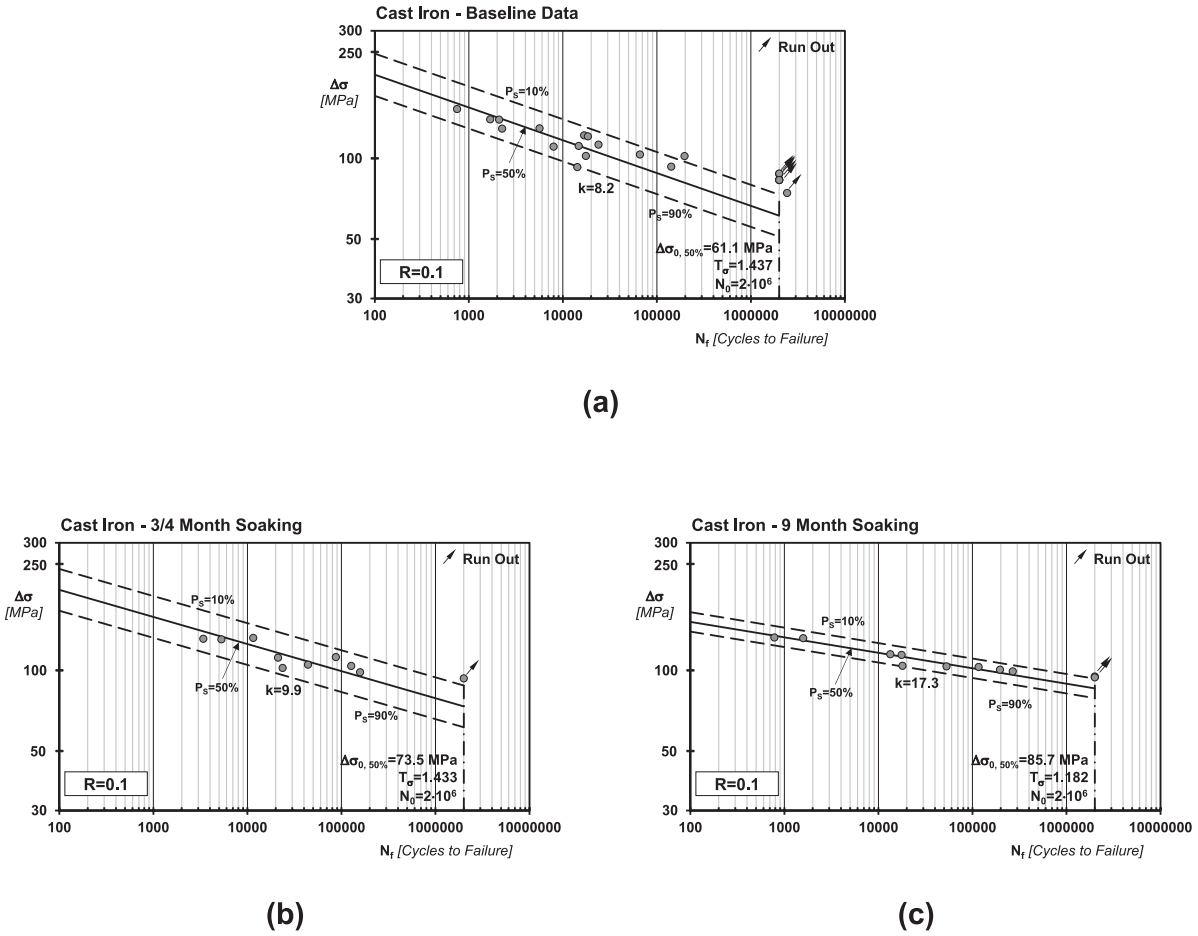

FIGURE 6 | Fatigue results generated by testing unsoaked (a) and hydrogen-soaked specimens (b, c) of cast iron.

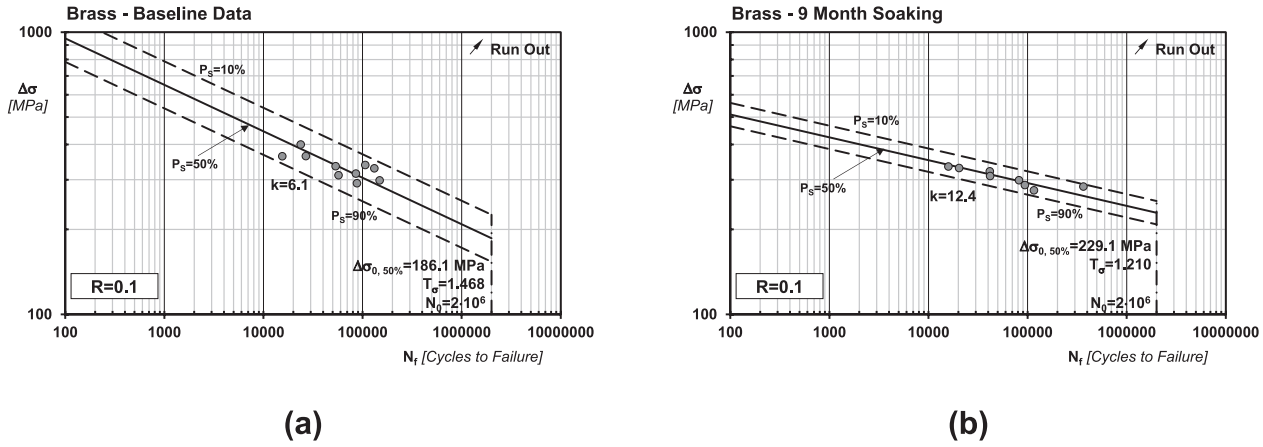

FIGURE 7 | Fatigue results generated by testing unsoaked (a) and hydrogen-soaked specimens (b) of brass.

Based on the results generated by testing as-received and soaked X52 steel welds, the most relevant considerations/outcomes are summarized as follows. The S–N curves for both as-received and hydrogen-soaked specimens (see Figure 5 and Table 1) exhibited exceptionally large negative inverse slopes, ranging from 14.7 to 46.6. These values significantly exceed the recommended value of 5 for fatigue assessment, as outlined in both Eurocode 3 [68] and the International Institute of Welding [69]. A notable increase in scatter was observed with longer soaking times, with the T_σ values being close to the commonly observed unifying value of 1.5 for fatigue curves of steel welded joints [70, 71].

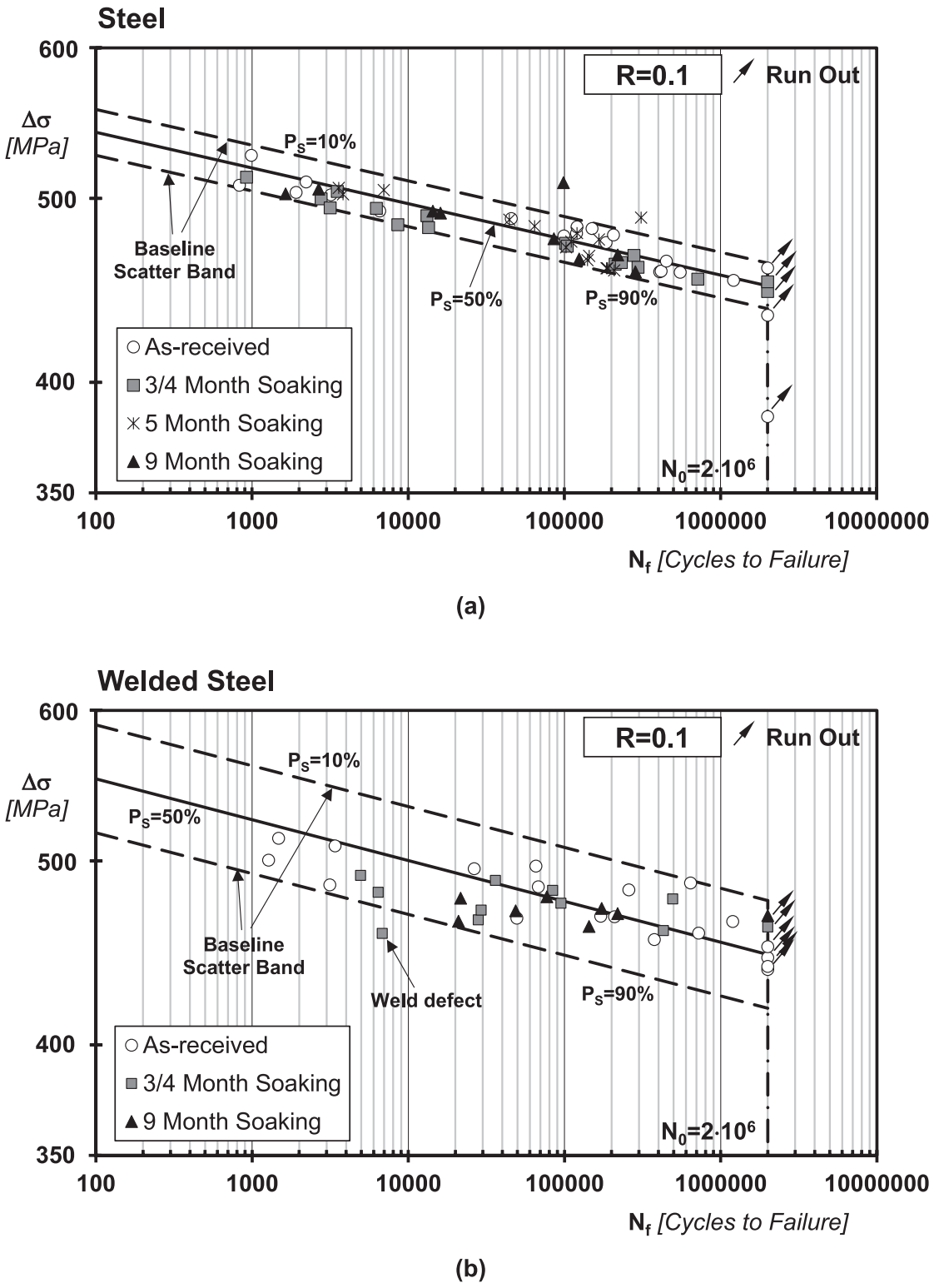

FIGURE 8 | Experimental results generated by testing soaked specimens versus baseline scatter band determined from specimens tested in the as-received condition for unwelded (a) and welded (b) X52 carbon steel.

The values reported in Table 1 reveal a decreasing trend in both $\Delta\sigma_{0,50\%}$ and k with increasing soaking time. This trend is particularly pronounced for the endurance limit, $\Delta\sigma_{0,50\%}$, which decreased by 18.6% after 9 months of soaking. The trends observed in Table 1 are influenced not only by the hydrogen soaking process but also by variations in sample size.

As far as cast iron is concerned (see Figure 6 and Table 1), the S–N curve for as-received specimens exhibited a negative inverse slope value typical of conventional metallic materials, falling within the range of 8–12 [67]. A slight decrease in scatter was observed with increasing soaking time, though this trend appears random and unrelated to any specific physical process. Table 1 reveals an increasing trend in both $\Delta\sigma_{0,50\%}$ and k with increasing soaking time, influenced by both the hydrogen soaking process and variations in sample size.

Similarly, for brass specimens (see Figure 7 and Table 1), the S–N curve for as-received specimens exhibited a negative inverse slope value typical of conventional metallic materials [67]. A slight decrease in scatter was also observed with increasing soaking time. The values reported in Table 1 indicate an increasing trend in both $\Delta\sigma_{0,50\%}$ and k with increasing soaking time, influenced by both the hydrogen soaking process and variations in sample size.

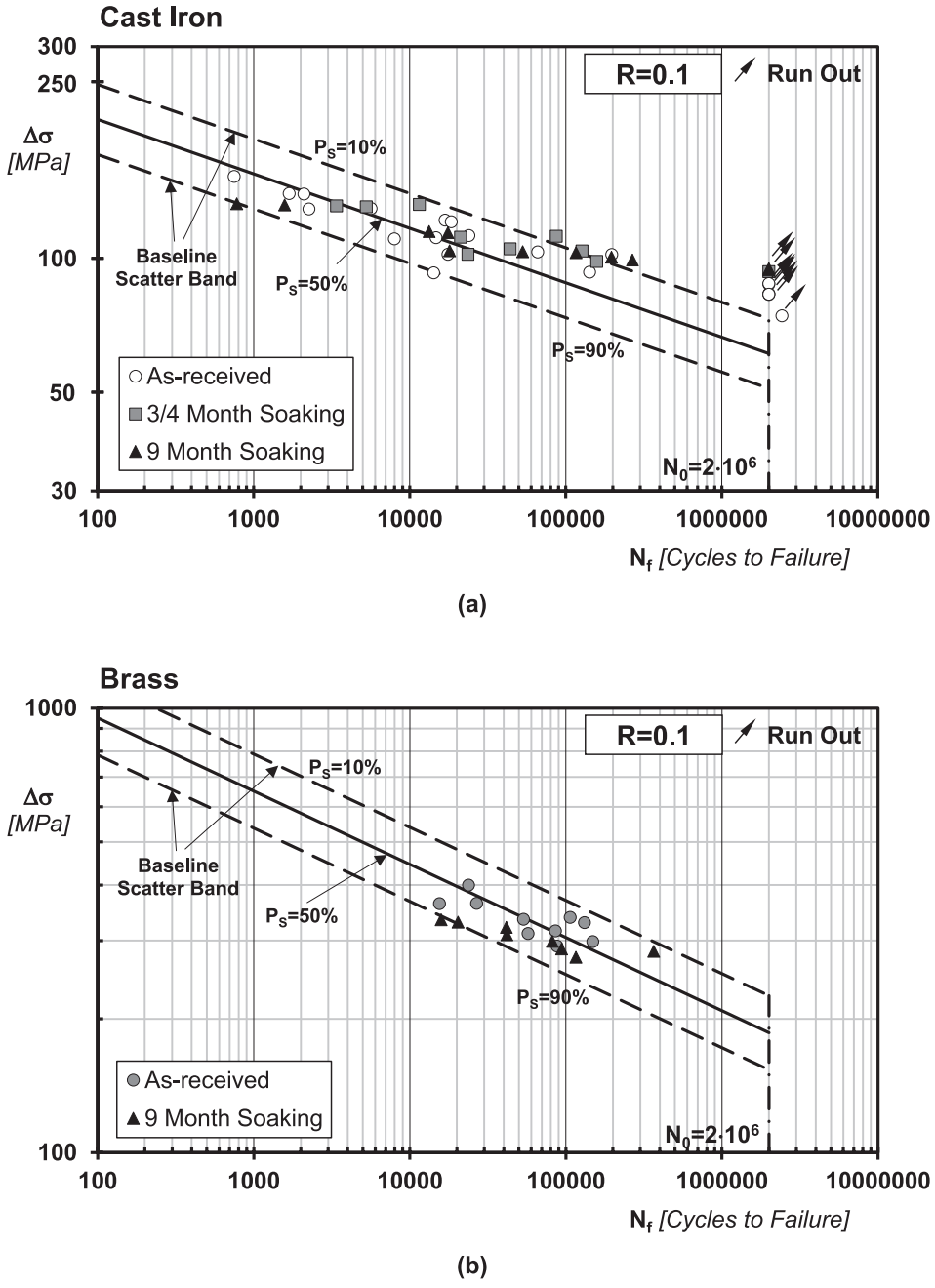

FIGURE 9 | Experimental results generated by testing soaked specimens versus baseline scatter band determined from specimens tested in the as-received condition for cast iron (a) and brass (b).

5 | Unsoaked Versus Hydrogen-Soaked Fatigue Behavior

In situ fatigue testing under hydrogen pressure better captures mechanisms such as oxide film fracture at the crack tip and stress-assisted hydrogen transport ahead of the crack, enabling continuous hydrogen absorption during propagation. Our ex situ approach, while not reproducing these dynamic effects, remains relevant for components that absorb hydrogen in service and are later fatigued without an external hydrogen source. Specifically, regarding crack initiation under fatigue loading, the detrimental effect of hydrogen is influenced by microstructural features, temperature, pressure, and loading frequency. While hydrogen appears to slightly affect medium-cycle fatigue behavior, its impact on high-cycle fatigue is negligible.

Based on these experimental findings, the fatigue testing protocol was designed with the following considerations. As structural elements in gas networks are pretensioned, both as-received and hydrogen soaked specimens were tested under a load ratio of 0.1. This load ratio allowed for the effective investigation of the combined effects of hydrogen and non-zero mean stresses. To focus on the low/medium cycle fatigue regime where hydrogen exhibits a more significant influence [35], fatigue tests were conducted in the range of 10^3–2×10^6 cycles to failure.

The rigorous statistical procedure recommended by the ASTM [64] was implemented to post-process the experimental results being generated. By assuming a log-normal distribution of the number of cycles to failure for each stress level and a 95% confidence level, the results were summarized in terms of negative inverse slope (k), endurance limit range ($\Delta\sigma_{0,50\%}$), and scatter ratio (T_σ).

The correlation between experimental results from soaked specimens and the corresponding baseline scatter bands, derived from as-received specimens, is illustrated in the S–N diagrams presented in Figures 8 and 9. These S–N diagrams demonstrate that the experimental results obtained from hydrogen-soaked specimens all fall within the baseline scatter band determined by postprocessing the results from as-received specimens. The only exception is the experimental point that falls outside the reference scatter band in Figure 8b. Further microstructure investigations showed that this point corresponds to a specimen containing a weld defect, which significantly reduced its fatigue life. However, as the aim of this investigation was to assess the fatigue behavior of metallic materials in the presence of hydrogen from a continuum mechanics perspective rather than a fracture mechanics approach, the effect of internal defects was not explored further. Nevertheless, since defects are a common issue in welded joints, the interplay between fatigue, hydrogen, and defects in weldments warrants further structured investigation.

The considerations discussed above suggest that, for the materials investigated, the hydrogen absorbed and trapped through the proposed experimental procedure had a negligible impact. This is confirmed by the fact that all experimental results for hydrogen-soaked specimens fall within the corresponding baseline scatter bands as seen in the S–N charts of Figures 8 and 9.

In terms of fatigue design, the implications of the last conclusion can be understood by recalling that, according to best practices for fatigue design and assessment [72–74], fatigue life is recommended to be estimated by referring to a fatigue curve determined experimentally for a probability of survival of at least 97.7%. Furthermore, the strength associated with this fatigue curve should be further penalized by adopting suitable safety factors, with the characteristics and values of these safety factors depending on the specific application. Accordingly, the design curve derived according to this procedure is characterized by an adequate level of safety. Recalling this common approach to fatigue assessment, it can be pointed out that the results generated by testing the hydrogen-soaked specimens are seen to fall within the corresponding 90%–10% scatter bands determined from as-received specimens. These findings suggest that, under the specific hydrogen-charging procedure and fatigue testing conditions adopted, safe fatigue life estimates can be obtained for the hydrogen-soaked specimens by adopting design curves determined by post-processing the results generated by testing the specimens in the as-received condition.

6 | Conclusions

In this work, the effect of hydrogen presoaking on the medium-cycle fatigue behavior of selected pipeline materials was systematically investigated using controlled exposure and statistical analysis. Based on the experimental findings, the following conclusions can be drawn for the specific hydrogen-charging procedure and fatigue testing conditions considered.

- Under the hydrogen presoaking conditions employed, absorbed hydrogen had only a negligible influence on the medium-cycle fatigue behavior of the tested materials.
- Both $\Delta\sigma_{0,50\%}$ and k vary with increasing soaking time.
- The variation *of* $\Delta\sigma_{0.50\%}$, k, and T_σ with soaking time is influenced by both the hydrogen soaking process and differences in sample size.
- The fatigue performance of hydrogen-soaked specimens remained within the scatter bands established for as-received specimens, suggesting that additional design allowances for hydrogen may not be necessary under similar pre-soaking conditions.
- These findings apply to ex situ testing after hydrogen exposure and do not capture mechanisms active during in situ fatigue under hydrogen pressure, where crack-tip oxide fracture and stress-assisted hydrogen transport can significantly influence crack propagation.

Nomenclature

k	negative inverse slope
N_f	number of cycles to failure

N_0 number of cycles to failure used to extrapolate the endurance limit

P_S probability of survival

R load ratio ($R = \sigma_{min}/\sigma_{max}$)

T_σ scatter ratio of the endurance limit range for 90% and 10% probabilities of survival

$\Delta\sigma$ stress range

$\Delta\sigma_0$ range of the endurance limit extrapolated at N_0

Author Contributions

E. Kufoin: investigation, data curation, formal analysis. **A. Bannister:** conceptualization, methodology, writing – review and editing. **M. Brown:** conceptualization, methodology, writing – review and editing. **D. Engelberg:** conceptualization, methodology, writing – review and editing, funding acquisition. **N. Kahlon:** conceptualization, methodology, writing – review and editing. **F. Scenini:** conceptualization, methodology, writing – review and editing, funding acquisition. **Y. Zhou:** investigation, writing – review and editing. **L. Susmel:** conceptualization, formal analysis, writing – original draft, writing – review and editing, supervision, funding acquisition.

Acknowledgments

The support of HSE (https://www.hse.gov.uk/) and the HyDeploy consortium (https://hydeploy.co.uk/) in funding the present research work is gratefully acknowledged. The contribution from Jonathan Duff for conducting the exposure in hydrogen environments is acknowledged. This work was also supported by the Henry Royce Institute for Advanced Materials, funded through EPSRC grants EP/R00661X/1 and EP/P025021/1.

Data Availability Statement

The data that support the findings of this study are available from the corresponding author upon reasonable request.

References

1. B. Reda, A. A. Elzamar, S. AlFazzani, and S. M. Ezzat, "Green Hydrogen as a Source of Renewable Energy: A Step Towards Sustainability, an Overview," *Environment, Development and Sustainability* 27 (2024): 29213–29233, https://doi.org/10.1007/s10668-024-04892-z.

2. J. B. Cristello, J. M. Yang, R. Hugo, Y. Lee, and S. S. Park, "Feasibility Analysis of Blending Hydrogen Into Natural Gas Networks," *International Journal of Hydrogen Energy* 48, no. 46 (2023): 17605–17629.

3. A. Islam, T. Alam, N. Sheibley, K. Edmonson, D. Burns, and M. Hernandez, "Hydrogen Blending in Natural Gas Pipelines: A Comprehensive Review of Material Compatibility and Safety Considerations," *International Journal of Hydrogen Energy* 93 (2024): 1429–1461.

4. L. Giannini, N. Razavi, A. Alvaro, and N. Paltrinieri, "Embrittlement, Degradation, and Loss Prevention of Hydrogen Pipelines," *MRS Bulletin* 49 (2024): 464–477.

5. A. Campari, F. Konert, O. Sobol, and A. Alvaro, "A Comparison of Vintage and Modern X65 Pipeline Steel Using Hollow Specimen Technique for In-Situ Hydrogen Testing," *Engineering Failure Analysis* 163, no. A (2024): 108530.

6. W. H. Johnson, "On Some Remarkable Changes Produced in Iron and Steel by the Action of Hydrogen and Acids," *Proceedings of the Royal Society of London* 23, no. 156–163 (1875): 168–179.

7. T. S. Sudarshan, M. R. Louthan, T. A. Place, and H. H. Mabie, "Role of Hydrogen and Humidity in the Torsional Fatigue of Aluminum Alloy 2024-T351," *Materials Science and Engineering* 73 (1985): 131–138.

8. H. Uyama, M. Nakashima, K. Morishige, Y. Mine, and Y. Murakami, "Effects of Hydrogen Charge on Microscopic Fatigue Behaviour of Annealed Carbon Steels," *Fatigue & Fracture of Engineering Materials & Structures* 29, no. 12 (2006): 1066–1074.

9. M. Kubota, N. Noyama, C. Sakae, and Y. Kondo, "Fretting Fatigue in Hydrogen Gas," *Tribology International* 39, no. 10 (2006): 1241–1247.

10. J. Capelle, J. Gilgert, and G. Pluvinage, "A Fatigue Initiation Parameter for Gas Pipe Steel Submitted to Hydrogen Absorption," *International Journal of Hydrogen Energy* 35, no. 2 (2010): 833–843.

11. M. Nakatani and K. Minoshima, "Influence of Activation Energy and Sensitivity to Hydrogen Embrittlement on Fatigue Strength Degradation by Irreversible Hydrogen in High-Strength Steels," *Fatigue & Fracture of Engineering Materials & Structures* 34 (2010): 363–373.

12. M. Kubota, K. Kuwada, Y. Tanaka, and Y. Kondo, "Mechanism of Reduction of Fretting Fatigue Limit Caused by Hydrogen Gas in SUS304 Austenitic Stainless Steel," *Tribology International* 44, no. 11 (2011): 1495–1502.

13. A. Macadre, H. Yano, S. Matsuoka, and J. Furtado, "The Effect of Hydrogen on the Fatigue Life of Ni–Cr–Mo Steel Envisaged for Use as a Storage Cylinder for a 70MPa Hydrogen Station," *International Journal of Fatigue* 33, no. 12 (2011): 1608–1619.

14. T. Michler, J. Naumann, and E. Sattler, "Influence of High Pressure Gaseous Hydrogen on S–N Fatigue in Two Austenitic Stainless Steels," *International Journal of Fatigue* 51 (2013): 1–7.

15. M. H. M. Kouters, H. M. Slot, W. van Zwieten, and J. van der Veer, "The Influence of Hydrogen on the Fatigue Life of Metallic Leaf Spring Components in a Vacuum Environment," *International Journal of Fatigue* 59 (2014): 309–314.

16. R. Komoda, M. Kubota, Y. Kondo, and J. Furtado, "Effect of Oxygen Addition on Fretting Fatigue Strength in Hydrogen of JIS SUS304 Stainless Steel," *Tribology International* 76 (2014): 92–99.

17. H. Matsunaga, M. Yoshikawa, R. Kondo, J. Yamabe, and S. Matsuoka, "Slow Strain Rate Tensile and Fatigue Properties of Cr–Mo and Carbon Steels in a 115 MPa Hydrogen Gas Atmosphere," *International Journal of Hydrogen Energy* 40, no. 16 (2015): 5739–5748.

18. G. Schauer, J. Roetting, M. Hahn, S. Schreijaeg, and S. Weihe, "Influence of Gaseous Hydrogen on Fatigue Behavior of Ferritic Stainless Steel—A Fatigue-Life Estimation," *Procedia Engineering* 133 (2015): 362–378.

19. J. A. Ronevich, B. P. Somerday, and C. W. San Marchi, "Effects of Microstructure Banding on Hydrogen Assisted Fatigue Crack Growth in X65 Pipeline Steels," *International Journal of Fatigue* 82, no. 3 (2016): 497–504.

20. T. Michler, J. Naumann, J. Wiebesiek, and E. Sattler, "Influence of Frequency and Wave Form on S-N Fatigue of Commercial Austenitic Stainless Steels With Different Nickel Contents in Inert Gas and in High Pressure Gaseous Hydrogen," *International Journal of Fatigue* 96 (2017): 67–77.

21. Y. Ogawa, H. Matsunaga, J. Yamabe, M. Yoshikawa, and S. Matsuoka, "Unified Evaluation of Hydrogen-Induced Crack Growth in Fatigue Tests and Fracture Toughness Tests of a Carbon Steel," *International Journal of Fatigue* 103 (2017): 223–233.

22. T. Shinko, G. Hénaff, D. Halm, G. Benoit, G. Bilotta, and M. Arzaghi, "Hydrogen-Affected Fatigue Crack Propagation at Various Loading Frequencies and Gaseous Hydrogen Pressures in Commercially Pure Iron," *International Journal of Fatigue* 121 (2019): 197–207.

23. T. An, S. Zhang, M. Feng, et al., "Synergistic Action of Hydrogen Gas and Weld Defects on Fracture Toughness of X80 Pipeline Steel," *International Journal of Fatigue* 120 (2019): 23–32.

24. N. Nagaishi, M. Yoshikawa, S. Okazaki, J. Yamabe, F. Yoshida, and H. Matsunaga, "Evaluation of Fatigue Life and Fatigue Limit of Circumferentially-Notched Type 304 Stainless Steel in Air and

Hydrogen Gas Based on Crack-Growth Property and Cyclic Stress-Strain Response," *Engineering Fracture Mechanics* 215 (2019): 164–177.

25. M. Kubota, M. Fukuda, and E. Komoda, "Effect of Hydrogen on Fatigue Limit of SCM435 Low-Alloy Steel," *Procedia Structural Integrity* 19 (2019): 520–527.

26. G. Pluvinage, J. Capelle, and M. Hadj Meliani, "Pipe Networks Transporting Hydrogen Pure or Blended With Natural Gas, Design and Maintenance," *Engineering Failure Analysis* 106 (2019): 104164.

27. A. Pradhan, M. Vishwakarma, and S. K. Dwivedi, "A Review: The Impact of Hydrogen Embrittlement on the Fatigue Strength of High Strength Steel," *Mater Today Proc* 26 (2020): 3015–3019.

28. J. Shang, W. Chen, J. Zheng, et al., "Enhanced Hydrogen Embrittlement of Low-Carbon Steel to Natural Gas/Hydrogen Mixtures," *Scripta Materialia* 189 (2020): 67–71.

29. W. Li, R. Cao, L. Xu, and L. Qiao, "The Role of Hydrogen in the Corrosion and Cracking of Steels—A Review," *Corrosion Communications* 4 (2021): 23–32.

30. X. Li, J. Yin, J. Zhang, et al., "Hydrogen Embrittlement and Failure Mechanisms of Multi-Principal Element Alloys: A Review," *Journal of Materials Science and Technology* 122 (2022): 20–32.

31. Y. Ogawa, H. Nishida, M. Nakamura, V. Olden, A. Vinogradov, and H. Matsunaga, "Dual Roles of Pearlite Microstructure to Interfere/Facilitate Gaseous Hydrogen-Assisted Fatigue Crack Growth in Plain Carbon Steels," *International Journal of Fatigue* 154 (2022): 106561.

32. C. Zhou, D. Tang, K. Zhang, et al., "Effect of Manganese Content on the Hydrogen Embrittlement of Twinning-Induced Plasticity (TWIP) Steels Under Hydrogen Charging and Hydrogen Environment," *Materials Science and Engineering a* 861, no. 19 (2022): 144289.

33. T. Zheng and N. Z. Chen, "A Cyclic Cohesive Zone Model for Predicting Hydrogen Assisted Fatigue Crack Growth (FCG) of Subsea Pipeline Steels," *International Journal of Fatigue* 173 (2023): 107707.

34. S. Yang, A. M. P. De Jesus, D. Meng, et al., "Very High-Cycle Fatigue Behavior of Steel in Hydrogen Environment: State of the Art Review and Challenges," *Engineering Failure Analysis* 166 (2024): 108898.

35. H. Wang, N. O. Larrosa, D. Engelberg, R. Best, and L. Susmel, "A Statistical Review of Hydrogen Effects on the Fatigue and Fracture Behaviour of Steel," *Fatigue & Fracture of Engineering Materials & Structures* 48, no. 9 (2025): 3613–3644.

36. L. Briottet, I. Moro, and P. Lemoine, "Quantifying the Hydrogen Embrittlement of Pipeline Steels for Safety Considerations," *International Journal of Hydrogen Energy* 37, no. 22 (2012): 17616–17623.

37. E. Summers, J. Race, M. A. Almoghayer, and D. Mignard, "A Review of the Challenges, Solutions and Economics of Hydrogen Transmission in Steel Pipelines," *JPSE* (in press), https://doi.org/10.1016/j.jpse.2026.100451.

38. H. Arashima, Y. Yanagisawa, R. ShigehitoIsobe, and N. Hashimoto, "Effects of Inclusions on the Fatigue Life of SNCM439 Steel in High-Pressure Hydrogen Gas," *International Journal of Hydrogen Energy* 47, no. 59 (2022): 25057–25065.

39. M. Sánchez, N. Marinova, E. Silveira, and N. Larrosa, "Standards and Codes for Hydrogen in Pipeline Infrastructure: Testing, Qualification, and Integrity Assessment," *Journal of Pipeline Science and Engineering* 5, no. 4 (2025): 100296.

40. A. Campari, F. Ustolin, A. Alvaro, and N. Paltrinieri, "A Review on Hydrogen Embrittlement and Risk-Based Inspection of Hydrogen Technologies," *International Journal of Hydrogen Energy* 48, no. 90 (2023): 35316–35346.

41. S. M. Lee, S. Y. Park, U. B. Baek, and B. H. Choi, "Evaluation of the Residual Fatigue Lifetime of a Semi-Elliptical Crack of a Low-Alloy Steel Pressure Vessel Under High-Pressure Gaseous Hydrogen," *International Journal of Fatigue* 176 (2023): 107875.

42. Q. Wang, J. Jiang, J. Dong, W. Chen, and J. Ye, "Fatigue Behavior and Life Prediction of Stainless Steels After Hydrogen Charging," *Structure* 85 (2026): 111205.

43. X. Wu, M. Teng, W. Jia, and J. Cai, "Study on the Mechanical Properties of X80 Pipeline Steel Under Pre-Charged High-Pressure Gaseous Hydrogen," *International Journal of Hydrogen Energy* 84, no. 26 (2024): 39–52.

44. P. Fernández-Pisón, L. M. Santana, Q. Sellam, V. Farrugia, Y. Madi, and J. Besson, "Oxygen-Mediated Inhibition of Gaseous Hydrogen Embrittlement in Pipeline Steels: Sub-Size Specimen Testing and Coupled Diffusion-Damage Modeling," *International Journal of Solids and Structures* 329 (2026): 113832.

45. M. Weihrauch, M. Patel, and E. A. Patterson, "Measurements and Predictions of Diffusible Hydrogen Escape and Absorption in Cathodically Charged 316LN Austenitic Stainless Steel," *Scientific Reports* 13 (2023): 10545.

46. T. Freitas, F. Konert, J. Nietzke, et al., "Tensile Testing in High-Pressure Gaseous Hydrogen Using the Hollow Specimen Method," *MRS Bulletin* 49 (2024): 1112–1120.

47. A. Zafra, G. Álvarez, G. Benoit, et al., "Hydrogen-Assisted Fatigue Crack Growth: Pre-Charging vs In-Situ Testing in Gaseous Environments," *Materials Science and Engineering a* 871, no. 26 (2023): 144885.

48. M. Röthig, J. Hoschke, C. Tapia, J. Venezuela, and A. Atrens, "A Review of Gas Phase Inhibition of Gaseous Hydrogen Embrittlement in Pipeline Steels," *International Journal of Hydrogen Energy* 60 (2024): 1239–1265.

49. D.-H. Lee, J. Y. Jung, K. H. Lee, et al., "Distinct Effects of In-Situ and Ex-Situ Hydrogen Charging Methods on the Mechanical Behavior of CoCrFeNi High-Entropy Alloy Fabricated by Laser-Powder Bed Fusion," *Journal of Alloys and Compounds* 940 (2023): 168858.

50. Y. Murakami and H. Matsunaga, "The Effect of Hydrogen on Fatigue Properties of Steels Used for Fuel Cell System," *International Journal of Fatigue* 28, no. 11 (2006): 1509–1520.

51. A. Arora, M. Singh, V. Nair, H. Singh, and D. K. Mahajan, "Role of Grain Size and Anisotropy of Neighboring Grains in Hydrogen-Assisted Intergranular Fatigue Crack Initiation in Austenitic Stainless Steel," *Fatigue and Fracture of Engineering Materials and Structures* 47 (2024): 3961–3979.

52. M. Bharati, R. Maity, A. Singh, and S. K. Paul, "The Fatigue Crack Growth Behavior of Hydrogenated 9Cr-1Mo Steel: An Experimental and Numerical Study," *Fatigue and Fracture of Engineering Materials and Structures* 47 (2024): 1677–1695.

53. Y. Zheng, H. Sun, L. Yan, X. Pang, and K. Gao, "Effect of Hydrogen on Very High Cycle Fatigue Properties of 17-4 PH Martensite Stainless Steel," *International Journal of Fatigue* 174 (2023): 107741.

54. L. Zhou, H. Zhang, Z. Yu, J. Wang, and H. Cui, "Hydrogen-Induced Fatigue Behavior of GH4169 Alloy: Experimentation and Crystal Plasticity Life Prediction Modeling," *International Journal of Hydrogen Energy* 193 (2025): 152356.

55. H. Wang, S. Cao, H. Ming, et al., "Insight Into the Hydrogen Permeation and Hydrogen Embrittlement Mechanisms of X52 Pipeline Steel Exposed to Gaseous Hydrogen," *International Journal of Hydrogen Energy* 133 (2025): 502–519.

56. A. M. Brass and F. Barbier, "Characterization of Hydrogen Permeation Through Recycled Cast Iron for Subsurface Disposal," *Journal of Nuclear Materials* 273 (1999): 265–270.

57. C. N. Panagopoulos and K. I. Giannakopoulos, "The Effect of Hydrogen Charging on the Mechanical Properties of Leaded α/β Brass Cast Alloy," *Materialia* 5 (2019): 100184.

58. Y. Sun and Y. F. Cheng, "Hydrogen-Induced Degradation of High-Strength Steel Pipeline Welds: A Critical Review," *Engineering Failure Analysis* 133 (2022): 105985.

59. Anon, "Standard Practice for Conducting Force Controlled Constant Amplitude Axial Fatigue Tests of Metallic Materials," ASTM E466, (2015).

60. W. D. Pilkey and D. F. Pilkey, *Peterson's Stress Concentration Factors*, 3rd ed., (John Wiley & Sons Inc., 2008).

61. M. A. Mohtadi-Bonab, "Effect of Different Parameters on Hydrogen Affected Fatigue Failure in Pipeline Steels," *Engineering Failure Analysis* 137 (2022): 106262.

62. L. B. Peral, A. Zafra, S. Blasón, C. Rodríguez, and J. Belzunce, "Effect of Hydrogen on the Fatigue Crack Growth Rate of Quenched and Tempered CrMo and CrMoV Steels," *International Journal of Fatigue* 120 (2019): 201–214.

63. Z. Lin, M. Wang, G. Sun, et al., "The Dependence of Fatigue Property on Applied Stress in X80 Pipeline Steel Notched Specimens in Hydrogen Gas Environment," *International Journal of Fatigue* 183 (2024): 108222.

64. ASTM E739-10, "Standard Practise for Statistical Analysis of Linear or Linearized Stress-Life (S-N) and Strain-Life (ε-N) Fatigue Data, ASTM," 2010, 1–7, https://doi.org/10.1520/E0739-23.2.

65. E. Kufoin and L. Susmel, "Quantitative Review of Probabilistic Approaches to Fatigue Design in the Medium Cycle Fatigue Regime," *Probabilistic Engineering Mechanics* 75 (2024): 103589.

66. E. Kufoin and L. Susmel, "On the Parametric Assessment of Fatigue Disparities," *Probabilistic Engineering Mechanics* 77 (2024): 103651.

67. L. Susmel, *Multiaxial Notch Fatigue: From Nominal to Local Stress-Strain Quantities* (Woodhead/CRC/Elsevier, 2009).

68. BS EN 1993-1-9:2025, "Eurocode 3: Design of Steel Structures—Part 1–9: Fatigue," British Standards Institution, 2025.

69. A. F. Hobbacher and J. Baumgartner, *Recommendations for Fatigue Design of Welded Joints and Components* (Springer Nature, 2024), https://doi.org/10.1007/978-3-031-57667-6.

70. E. Haibach, *Service Fatigue-Strength—Methods and Data for Structural Analysis* (VDI, 1992).

71. L. Susmel, C. M. Sonsino, and R. Tovo, "Accuracy of the Modified Wöhler Curve Method Applied Along With the $r_{ref} = 1$ mm Concept in Estimating Lifetime of Welded Joints Subjected to Multiaxial Fatigue Loading," *International Journal of Fatigue* 33 (2011): 1075–1091.

72. R. W. Hertzberg, *Deformation and Fracture Mechanics of Engineering Materials*, 4th ed., (Wiley, 1996).

73. Y.-L. Lee, J. Pan, R. Hathaway, and M. Barkey, "Fatigue Testing and Analysis," in *Butterworth-Heinemann* (Elsevier, 2005).

74. C. M. Sonsino, "Course of SN-Curves Especially in the High-Cycle Fatigue Regime With Regard to Component Design and Safety," *International Journal of Fatigue* 29, no. 12 (2007): 2246–2258.

75. Y.-L. Lee, J. Pan, R. Hathaway, and M. Barkey, *Fatigue Testing and Analysis* (Elsevier, 2005).

76. M. Gibbons Natrella, "Experimental Statistics," National Bureau of Standards, Handbook 91, (1963).

Appendix A

Statistical Derivation of Fatigue Curves

In a log–log representation (Figure A1), fatigue curves are commonly approximated by straight lines and can therefore be expressed using the following classical Wöhler-type relationship:

$$\Delta\sigma^{k} \cdot N_f = \Delta\sigma_0^{k} \cdot N_0 \tag{A1}$$

where $\Delta\sigma_0$ denotes the endurance limit extrapolated at N_0 cycles to failure.

In practice, fatigue curves are typically obtained by means of a linear least squares regression, carried out under the assumption that the number of cycles to failure follows a log-normal distribution at any given stress range (Figure A1) [65]. On this basis, for a given experimental dataset, the median (50% probability of survival) fatigue curve is identified by estimating the constants C_0 and C_1 in the following linear regression model:

$$\log N_f = C_0 + C_1 \cdot \log \Delta\sigma \tag{A2}$$

in which $\Delta\sigma$ is treated as the independent variable and N_f as the dependent variable.

Let the number of experimental points used to fit Equation (A2) be n. For the i-th specimen ($i = 1, 2, ..., n$), the applied stress range is $\Delta\sigma_i$ and the corresponding measured number of cycles to failure is $N_{f,i}$. Using the least squares criterion, the regression coefficients C_0 and C_1 can be computed as follows [75]:

$$C_1 = \frac{\sum_{i=1}^{n} \left(\log \Delta\sigma_i - x_m\right) \cdot \left(\log N_{f,i} - y_m\right)}{\sum_{i=1}^{n} \left(\log \Delta\sigma_i - x_m\right)^2} \tag{A3}$$

$$C_0 = y_m - C_1 \cdot x_m \tag{A4}$$

with

$$x_m = \frac{\sum_{i=1}^{n} \log \Delta\sigma_i}{n}; y_m = \frac{\sum_{i=1}^{n} \log N_{f,i}}{n} \tag{A5}$$

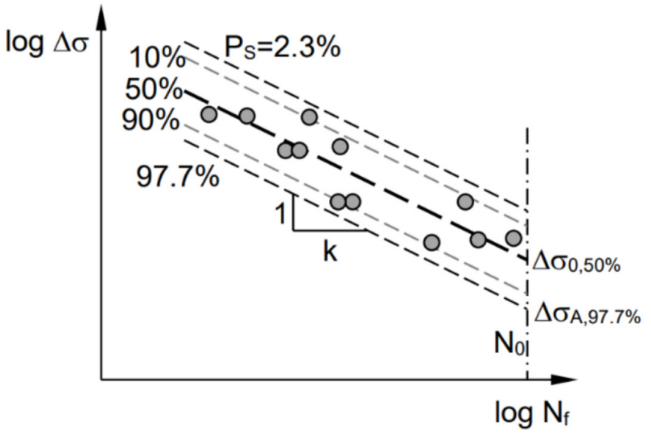

FIGURE A1 | Log–log S–N diagram and S–N curves constructed for different probabilities of survival. [Colour figure can be viewed at wileyonlinelibrary.com]

Once C_0 and C_1 are determined, the negative inverse slope k and the endurance limit $\Delta\sigma_{0,50\%}$ extrapolated at N_0 cycles to failure for a 50% probability of survival can be obtained by rewriting Equation (A1) in the form of Equation (A2), which yields the following:

$$k = -C_1;\ \Delta\sigma_{0,50\%} = \left(\frac{10^{C_0}}{N_0}\right) \tag{A6}$$

To characterize the scatter of the experimental results, the corresponding standard deviation is first evaluated using the following conventional expression:

$$s = \sqrt{\frac{\sum_{i=1}^{n}\left[\log N_{f,i} - \log N_0\left(\frac{\Delta\sigma_{0,50\%}}{\Delta\sigma_i}\right)^2\right]^2}{n-1}} \tag{A7}$$

The standard deviation s can then be used to estimate the endurance limit at N_0 cycles to failure for probabilities of survival equal to P% and (1 − P)%, respectively (Figure A1), namely,

$$\Delta\sigma_{0,P\%} = \Delta\sigma_{0,50\%} \cdot \left[\frac{N_0}{10^{\log(N_0)+q\cdot s}}\right]^{\frac{1}{k}} \tag{A8}$$

$$\Delta\sigma_{0,(1-P)\%} = \Delta\sigma_{0,50\%} \cdot \left[\frac{N_0}{10^{\log(N_0)-q\cdot s}}\right]^{\frac{1}{k}} \tag{A9}$$

In Equations (A8) and (A9), q is a statistical factor that depends on the selected confidence level, the target probability of survival, and the sample size [72, 76].

Finally, it is important to note that the curves corresponding to probabilities of survival P% and (1 − P)% share the same negative inverse slope k as the median (50%) Wöhler curve, as given by Equation (A6).